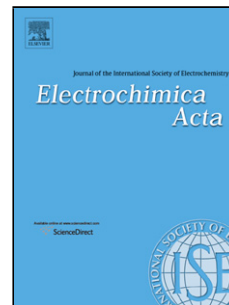


Accepted Manuscript

Title: Characterization of PEDOT-Quinone Conducting Redox Polymers for Water Based Secondary Batteries

Authors: Mia Sterby, Rikard Emanuelsson, Xiao Huang, Adolf Gogoll, Maria Strømme, Martin Sjödín



PII: S0013-4686(17)30534-0
DOI: <http://dx.doi.org/doi:10.1016/j.electacta.2017.03.068>
Reference: EA 29102

To appear in: *Electrochimica Acta*

Received date: 19-12-2016
Revised date: 8-3-2017
Accepted date: 8-3-2017

Please cite this article as: Mia Sterby, Rikard Emanuelsson, Xiao Huang, Adolf Gogoll, Maria Strømme, Martin Sjödín, Characterization of PEDOT-Quinone Conducting Redox Polymers for Water Based Secondary Batteries, *Electrochimica Acta* <http://dx.doi.org/10.1016/j.electacta.2017.03.068>

This is a PDF file of an unedited manuscript that has been accepted for publication. As a service to our customers we are providing this early version of the manuscript. The manuscript will undergo copyediting, typesetting, and review of the resulting proof before it is published in its final form. Please note that during the production process errors may be discovered which could affect the content, and all legal disclaimers that apply to the journal pertain.

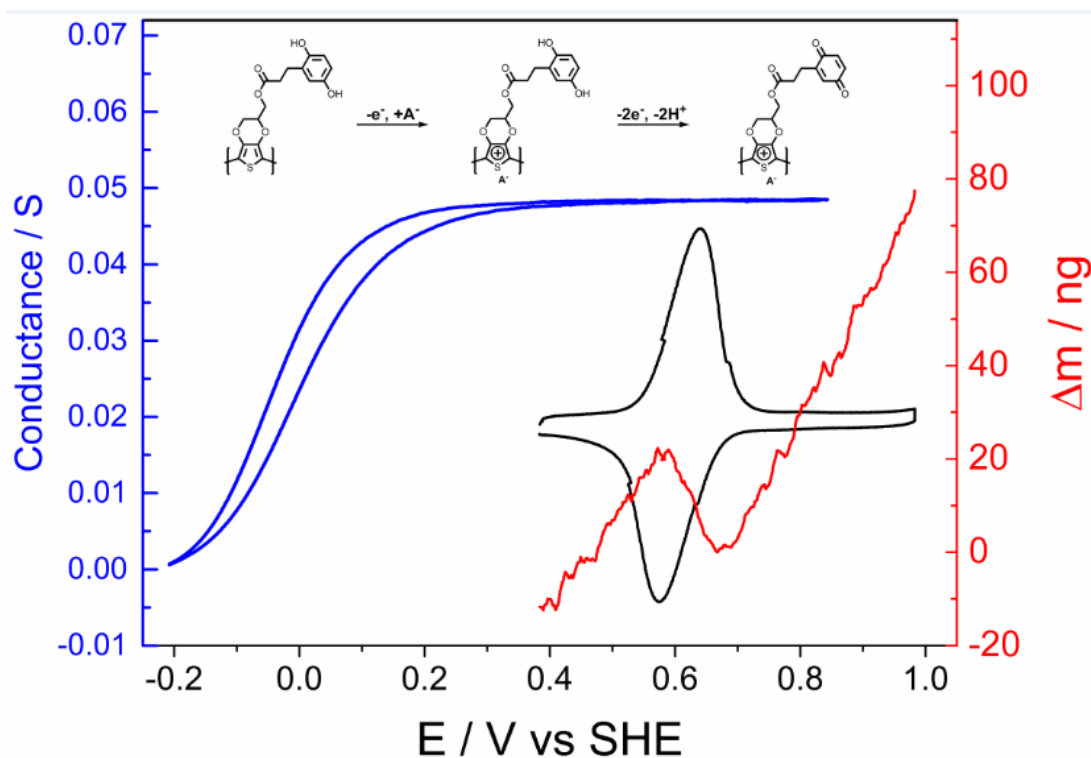
Characterization of PEDOT-Quinone Conducting Redox Polymers for Water Based Secondary Batteries

Mia Sterby,^a Rikard Emanuelsson,^a Xiao Huang,^b Adolf Gogoll,^b Maria Strømme,^a and Martin Sjödin^a

^a Nanotechnology and Functional Materials, Department of Engineering Sciences, The Ångström Laboratory, Uppsala University, Box 534, SE-751 21 Uppsala, Sweden

^b Department of Chemistry - BMC, Biomedical Centre, Uppsala University, Box 576, SE-751 23 Uppsala, Sweden

Graphical abstract



Abstract

Lithium-ion technologies show great promise to meet the demands that the transition towards renewable energy sources and the electrification of the transport sector put forward. However, concerns regarding lithium-ion batteries, including limited material resources, high energy consumption during production, and flammable electrolytes, necessitate research on alternative technologies for electrochemical energy storage. Organic materials derived from abundant building blocks and with tunable properties, together with water based electrolytes, could provide safe, inexpensive and sustainable alternatives. In this study, two conducting redox polymers based on poly(3,4-ethylenedioxythiophene) (PEDOT) and a hydroquinone pendant group have been synthesized and characterized in an acidic aqueous electrolyte. The polymers were characterized with regards to kinetics, pH dependence, and mass changes during oxidation and reduction, as well as their conductance. Both polymers show redox matching, i.e. the quinone redox reaction occurs within the potential region where the polymer is conducting, and fast redox conversion that involves proton cycling during pendant group redox conversion. These properties make the presented materials promising candidates as electrode materials for water based all-organic batteries.

Keywords: Conducting Redox Polymer, Quinone, Organic Batteries, Proton Batteries, Redox Matching

1 Introduction

The need for electrical energy storage (EES) is steadily increasing and with that comes increased requirements on EES technologies regarding safety, sustainability and reduced environmental impact. Currently, the most promising EES-system that could meet future energy storage demands is based on the lithium-ion technology. The primary concerns with current lithium-ion batteries (LIBs) are linked to safety due to flammable electrolytes [1], high costs, high energy consumption in their production and limited material resources due to the lithium metal oxide materials used as cathodes [2, 3]. Commercially available LIBs are using electrolytes containing mixtures of organic carbonates [4] which are flammable and/or harmful. Future EES technologies would benefit from using non-flammable and non-harmful electrolytes and to avoid the use of organic solvents, aqueous systems could be used.

Commercial LIBs have a cell voltage of around 3.8 V and the voltage of a water based EES systems is limited by the water stability window of 1.23 V. However, Suo et al. have recently increased the stability window of aqueous electrolytes to ~3.0 V using highly concentrated salt solutions, enabling water based EES systems to operate at voltages approaching that of LIBs [5].

Existing cathode materials most often include rare and expensive metals with high molecular weights (e.g. cobalt, manganese, and nickel) that are extracted through energy-intensive mining [6]. Organic materials, with their inexpensive, abundant and readily available building blocks (H C O N S) and tunable properties, have therefore been proposed as replacements for inorganic cathode materials [7, 8]. Many organic battery materials have previously been studied, including carbonyl compounds [9, 10], conducting polymers [11-13], radicals [14-16], and organosulfur compounds [7, 17, 18]. A unique class of carbonyl compounds that has been extensively studied in the field of organic matter based EES is constituted by the

quinones. Quinones are naturally occurring and they are involved in e.g. the electron transport chains of photosynthesis and respiration [19]. Their high discharge capacity [9, 20, 21] and reversible redox chemistry [21, 22], both in organic solvent and in aqueous solution, make them attractive as components in EES applications. Moreover, quinones offer the possibility of introducing various functional groups through chemical substitution, which allows for tuning of the quinone physical properties. In particular the possibility to adjust the quinone redox potential by substitution is of essence for the development of battery materials. Batteries using quinones as anode and cathode material in the same device have been demonstrated by virtue of this substitution induced voltage tuning [8, 23]. However, quinones show low electronic conductivity and are easily dissolved in the electrolyte [24-26].

To solve these problems the quinone can be connected to a conducting polymer forming a conducting redox polymer (CRP). A CRP consists of a conducting polymer backbone, a redox active pendant group which can store charge, and a linker connecting the pendant group to the backbone (Figure 1).

These types of battery materials have previously been investigated [27, 28]. They allow for organic battery electrodes with both good conductivity, without the use of carbon additives, and high charge storage capacity. In a CRP the conducting polymer backbone serves to provide an electronic conductivity path through the material while the purpose of the pendant group is to provide a well-defined redox reaction and a high charge storage capacity. That is, the individual, unperturbed, properties of the conducting polymer and the redox group are desirable in the CRP material. Moreover, as conducting polymers are only conducting when in their oxidized or reduced states, i.e. in their doped states, the quinone redox reaction has to occur in a potential region where the polymer is doped in order to benefit from polymer conductivity, a condition referred to as redox matching.

In a previous study with polypyrrole (PPy) as polymer backbone and a quinone pendant group, the polymer conductivity was severely compromised by the redox activity of the quinone [29]. This was concluded to be due to a twisting of the PPy backbone upon oxidation of the quinone group, resulting in a localization of charge carriers. In the PPy-quinone system the requirement for unperturbed properties of the active moieties was thus not met. In this study we use the more rigid poly(3,4-ethylenedioxythiophene) (PEDOT) backbone, which potentially can withstand the forces imposed on the polymer backbone during hydroquinone to quinone redox conversion. The quinone functional groups are attached covalently to the PEDOT backbone via two different linkers, thus forming two different CRPs (monomers shown in Figure 2). We show that in these polymers the requirement of redox matching is met and that the conductance of the polymer backbone is largely unaffected by the pendant group. We also discuss the electrochemical characteristics of the materials within the framework of cathode materials for water based quinone batteries.

2 Experimental

All reagents were purchased from Sigma-Aldrich and were used without further purifications unless otherwise specified. Acetonitrile was dried over molecular sieves prior to use and deionized water was used to prepare aqueous electrolytes. All electrochemical experiments were conducted at ambient temperature and the electrolyte solutions were purged with N₂ prior to measurements. Electrochemical measurements were performed on an Autolab PGSTAT302N potentiostat (Ecochemie, The Netherlands) equipped with a bipotentiostat module except for electrochemical quartz crystal microbalance (EQCM) measurements that were performed on a VersaSTAT 3 potentiostat/galvanostat (Princeton Applied Research, USA) together with a QCM922A quartz crystal microbalance (Princeton Applied Research,

USA). All potentials are reported vs. standard hydrogen electrode (SHE) unless otherwise specified.

2.1 Monomer synthesis

Nuclear magnetic resonance (NMR) spectra were recorded on an Agilent MR (^1H at 399.97 MHz, ^{13}C at 100.58 MHz) spectrometer. Chemical shifts are reported in ppm relative to tetramethylsilane (TMS) *via* the residual solvent signals: CDCl_3 , ^1H at 7.26 and ^{13}C at 77.0 ppm. The following abbreviations were used: s = singlet, d = doublet, t = triplet, q = quartet, m = multiplet, dd = doublet of doublets, and br = broad. Solvents for extraction and chromatography were of technical grade and were used without further purification. Flash chromatography was performed using silica gel (200 \pm 300 mesh). For mass spectra, samples were dissolved in a mixture of water:methanol:formic acid 49:50:1, and 10 μL of this solution was introduced *via* spray needle into an LTQ Orbitrap Velos Pro ETD mass spectrometer using a spray voltage of 1.8 kV in the m/z range 100-1200. The resolution in the Fourier Transform analyzer (Orbitrap) was 60 000. Spectra were collected for 2-3 min. Microwave heating was performed with an Initiator+ microwave system (Biotage). See Supplementary Figures S1-S7 for characterization spectra of **M1**.

2.1.1 M1 Synthesis

Bromohydroquinone (20 g, 0.106 mol) and 3,4-dihydro-2H-pyran (DHP) (50 mL) were stirred in a round-bottom flask. Trifluoroacetic acid (TFA, 2-4 drops) was added to the mixture and the solution was stirred at room temperature for 15 h. The reaction mixture was diluted with diethyl ether (50 mL) and then poured into aqueous NH_4Cl solution (saturated, 50 mL). After separation the organic layer was dried over MgSO_4 . The solvent was removed under vacuum and the crude product was purified by chromatography (SiO_2 , pentane/ethyl acetate, 10/1) yielding **1** as a white solid (33.32 g, 88%).

^1H NMR (CDCl_3), δ = 7.28 (1H, dd, J = 2.8, 1.6 Hz), 7.06 (1H, dd, J = 9.0, 1.6 Hz), 6.94 (1H, dd, J = 9.0, 2.8 Hz), 5.36 (1H, dt, J = 3.2, 3.1 Hz), 5.30 (1H, dt, J = 3.1, 2.6 Hz), 3.92 (2H, m), 3.59 (2H, m), 2.07 (1H, m), 1.96 (2H, m), 1.90-1.80 (3H, m), 1.75-1.54 (6H, m).

^{13}C NMR (CDCl_3), δ = 152.20, 152.17, 148.4, 148.3, 121.5, 121.4, 117.9, 117.8, 116.5, 116.4, 113.49, 113.48, 97.6, 97.5, 97.2, 97.1, 62.0, 61.8, 30.31, 30.3, 30.24, 30.23, 25.3, 25.2, 18.67, 18.66, 18.42, 18.41 (Three diastereomers should give 48 signals, but due to overlapping peaks only 28 are distinguishable).

m.p.: 65 °C.

HRMS, calculated for $\text{C}_{16}\text{H}_{21}\text{O}_4\text{Na}^+$: m/z = 379.0515, found: m/z = 379.0514.

Thiophene derivative **2** was prepared according to the procedure previously reported [30]. A mixture of THP-protected 2-bromohydroquinone **1** (180 mg, 0.504 mmol), **2** (100 mg, 0.554 mmol), $\text{Pd}(\text{PPh}_3)_2\text{Cl}_2$ (18 mg, 0.025 mmol), CuI (5 mg, 0.025 mmol), triphenylphosphine (26 mg, 0.101 mmol), diethylamine (0.8 mL, 7.73 mmol), and dimethylformamide (0.5 mL) was stirred under nitrogen atmosphere in a heavy-walled glass Smith process vial at 120 °C for 25 min in the microwave cavity. The reaction mixture was then treated with diethyl ether, filtered, and poured into 0.1 M aqueous HCl (5-10 mL). The organic layer was collected and washed with brine (2×15 mL). It was then dried over MgSO_4 and condensed under vacuum. Following purification by chromatography (SiO_2 , pentane/ethyl acetate, 10/1), the crude product **3** (100 mg) was used directly in the next step. After dissolution in a solvent mixture (methanol/DCM, 2 mL/3 mL), TFA (2 drops) was added and the mixture was stirred at room temperature for 12 h. Aqueous NaHCO_3 (saturated, 2 mL) was added to the mixture that was then separated between DCM and water. The organic layer was collected and dried over MgSO_4 . After removing the organic solvent under vacuum the crude substrate was purified by

chromatography (SiO₂, pentane/ethyl acetate, 2/1), yielding **M1** as a waxy yellow solid (50 mg, 35 %). The synthetic route is summarized in Scheme 1.

¹H NMR (CDCl₃), δ = 6.80 (1H, d, J = 8.7 Hz), 6.77 (1H, d, J = 3.1 Hz), 6.73 (1H, dd, J = 8.7, 3.1 Hz), 6.39 (1H, d, J = 3.8 Hz), 6.36 (1H, d, J = 3.8 Hz), 5.63 (1H, br s), 4.80 (1H, br s), 4.40 (1H, m), 4.30 (1H, dd, J = 11.7, 2.2 Hz), 4.10 (1H, dd, J = 11.7, 7.1 Hz), 2.92 (1H, dd, J = 17.2, 6.3 Hz), 2.85 (1H, dd, J = 17.2, 7.0 Hz).

¹³C NMR (CDCl₃), δ = 151.3, 148.6, 141.1, 141.0, 117.8, 117.4, 115.5, 109.6, 100.2, 100.0, 91.2, 77.7, 71.6, 67.2, 22.1.

m.p.: 39 °C.

HRMS calculated for C₁₅H₁₃O₄S⁺: m/z = 289.0529, found: m/z = 289.0527.

2.1.2 M2 Synthesis

Monomer **M2** was synthesized as previously reported [31] i.e. carboxylic acid **4** was reacted with BBr₃ in DCM at 0 °C, forming **5** and subsequently treated with NaOH to form **6**. The crude **6** was mixed with EDOT-MeBr and KHCO₃ in anhydrous DMF and heated at 85 °C, yielding **M2**. The synthetic route is summarized in Scheme 2.

2.2 Polymerization

All polymerizations were performed using cyclic voltammetry where the potential was cycled between -0.3 and 1.1 V (vs. Fc^{0/+}) at 100 mV/s (25 mV/s for interdigitated array (IDA) measurements). The number of cycles varied between 1 and 13. The organic electrolyte used for polymerization was tetrabutylammonium hexafluorophosphate (TBAPF₆, 0.1 M) in dry acetonitrile (MeCN). A platinum wire was used as counter electrode and a Ag/Ag⁺ (10 mM AgNO₃, 0.1 M TBAPF₆, -0.096 V vs. Fc^{0/+}) electrode in a separate compartment was used as

reference. Polymerizations were performed with a monomer concentration of 5 mM. After polymerization the electrode was washed with MeCN and water. For EQCM measurements the monomers were polymerized on a gold coated AT-cut quartz EQCM-crystal (8.95 MHz \pm 30 kHz, \varnothing 5 mm) while the working electrode for IDA measurements was an IDA-electrode with 90 pairs of Au bands on glass substrate (10 μ m between bands, 150 nm high, MicruX Technologies, Spain). For Scanning Electron Microscopy (SEM) images the monomers were electropolymerized onto a graphite paper. For all other experiments a glassy carbon (GC) electrode (3.0 mm diameter, BASi, USA) was used as working electrode.

2.3 Electrochemical Characterization

The polymers were characterized by cyclic voltammetry in aqueous electrolyte with 1 M sodium nitrate buffered with sodium acetate, monobasic sodium phosphate, and boric acid (0.1 M each). A platinum wire was used as counter electrode and a Ag/AgCl (3 M NaCl, +0.192 V vs. SHE) electrode was used as reference. The pH was adjusted with concentrated HNO₃ or NaOH_{aq} and voltammograms were measured over the pH interval 0 to 10 for both polymers at a scan rate of 10 mV/s. To obtain kinetic information, cyclic voltammetry experiments at various scan rates, between 1 mV/s and 30 V/s, were performed. In these experiments as well as for EQCM experiments the pH was adjusted to 0. Conductance measurements were performed in situ during cyclic voltammetry as previously reported [32] using a bipotentiostat with a voltage bias between the two working electrodes of 1mV for polymerization and 10 mV for characterization. The conductance of the polymer was determined from the bias voltage and the current passing between the two working electrodes. The current, in turn, was evaluated from the sum of the absolute current responses (divided by two in order to avoid double counting) from the two electrodes during the voltammetry experiment. In order to expand the stability window of the electrolyte a “water-in-salt”

electrolyte [5] was used consisting of a sodium chloride and hydrochloric acid (1 M) salt slurry. SEM images were obtained using a Leo Gemini 1550 FEG SEM instrument (Zeiss, Germany) operated at 7 kV with an in-lens secondary electron detector. No sputtering was performed on the polymers prior to imaging as the material was found to be sufficiently conducting to prevent charging.

3 Results and Discussion

3.1 Polymerization

During electropolymerization the irreversible oxidation peak seen above ~ 0.8 V (vs. $\text{Fc}^{0/+}$) (Figure 3) is related to polymer formation. For each scan an increased current at low potentials can be seen that corresponds to an increased capacitive charge due to polymer doping. The semi-reversible redox reaction centered at 0.34 V for polymer **P1** and 0.36 V for polymer **P2** corresponds to the redox chemistry of the pendant group, showing a buildup of quinone moieties concurrently with the polymer formation.

3.2 SEM Analysis

From the SEM images (Figure 4) of electropolymerized **P1** and **P2**, open morphologies for both CRPs can be seen with polymer grains aggregated to web-like structures. The grains have diameters of about 500 nm and are separated by micrometer-sized pores. Since both solvent molecules and the ions used in the electrochemical characterization experiments have radii in the low-nm range and the pore size is around 1 μm both solvent molecules and ions should easily be able to penetrate into the polymer pore structure. Moreover, since both polymers show similar morphologies, no difference between the two polymers are expected with respect to solvent and ion accessibility.

3.3 Cyclic Voltammetry

The cyclic voltammograms (CVs) of polymers **P1** and **P2**, seen in figure Figure 5a and Figure 5b respectively, are dominated by the chemically reversible hydroquinone/quinone redox conversion peak centered at 0.70 V (for **P1**) and 0.63 V (for **P2**). In addition to the quinone peak a capacitance increase, as compared to the bare electrode, can be seen at potentials on both sides of the quinone peak. We attribute this capacitance to the doping of the PEDOT backbone that is expected to provide a relatively featureless capacitance extending over the entire potential interval studied, as judged from the CV of pristine PEDOT (dotted lines Figure 5). Assuming a constant capacitance from the PEDOT backbone in the potential interval investigated, the capacitance originating from the backbone was evaluated for **P1** to 12 % of the total capacity and the remaining 88 % from the pendant group redox activity. For **P2** the capacitance originating from the backbone was evaluated to 22 % of the total capacity and the remaining 78 % from the pendant group redox activity. **P1** shows a slightly broader quinone peak and a larger peak separation compared to **P2** (**P1** has a peak split of 75 mV and **P2** has a peak split of 16 mV, at 25 mV/s), which agrees with a lower apparent rate constant for **P1** (vide infra).

3.4 Kinetics

At scan rates (ν) below 0.1 V/s the oxidation and reduction peak currents (i_p) increase linearly with scan rate and a plot of $\ln(i_p)$ against $\ln(\nu)$ (Supplementary Figure S8) yields a linear dependence with a slope of 1, indicating a reaction which is not diffusion-limited at these scan rates. At higher scan rates, above 1 V/s, the oxidation and reduction peak potentials drift apart. From the scan rate dependence of the peak potentials apparent rate constants (k^0) can be calculated using Equation 1 [33, 34],

$$E_p = E^{0'} \pm \frac{RT}{\alpha z F} \times \ln \left(\frac{\alpha z F \nu}{RT k^0} \right) \quad (1)$$

where α is the transfer coefficient, z is the number of charges transferred, and $E^{0'}$ is the formal potential and where the plus sign signifies reduction and the minus sign oxidation. The apparent rate constants were calculated from the linear regions (inset in Figure 6a) to 7.8 s^{-1} (oxidation) and 6.4 s^{-1} (reduction) for **P1**. For **P2** the apparent rate constants were determined to 20.3 s^{-1} (oxidation) and 26.7 s^{-1} (reduction) (see inset in Figure 6b). Both polymers show fast kinetics compared to other battery materials, which might be partially due to the open structures of the polymers (Figure 4) that allow for fast mass transport through the material. It should, however, be noted that the polymers are both thin films (thickness in the low micrometer range) and thus cannot be compared directly with most commercially available battery materials. The rate constants for **P2** are higher than those for **P1** indicating faster kinetics. This can also be perceived from the CVs (Figure 5), where the redox peaks for **P2** are significantly narrower than those for **P1**. When increasing the scan rate the redox peaks move apart and are broadened, which could either be due to mass transfer limitations or sluggish redox conversion of the pendant group. The absence of a diffusion tail even at high scan rates for both **P1** and **P2** (Figure 6) suggests that diffusion is not rate limiting, even at scan rates above 1 V/s , and hence that the reaction must be limited by electron transfer. As the two monomers building up the polymers differ only with respect to the linker it is tempting to attribute the difference in rate constant to a rate limiting electron transfer between the pendant and the polymer backbone. It is however unclear why the longer aliphatic linker in **P2** should be more favorable for fast electron transport than the short alkyne linker in **P1**. Alternatively, the difference in rate might be due to subtle differences in polymer morphology. Noriega et al. suggested that fast charge transport in conjugated polymers can be achieved in disordered

materials through interconnected ordered regions in a predominantly amorphous matrix [35]. For the polymers in this work, i.e. CRPs, electron transfer between the ordered regions, where charge transport predominantly occurs, and amorphous regions is required for full redox-conversion of the material. We suggest that this electron transfer reaction is rate limiting and hence that the difference in rate constants is due to the variations in the barriers or orbital overlap involved in electron transport between amorphous and ordered regions of the material.

3.5 pH-Dependence

The formal potential (E^0) of the quinone reduction depends heavily on pH for both **P1** and **P2**. In the pH-interval between 0 and 10 (Figure 7, CVs for different pH of **P1** in Figure S9 and of **P2** in Figure S10) a slope of -61 mV/pH was seen for **P1** and a slope of -59 mV/pH was seen for **P2**. This indicates proton coupled redox reactions for both **P1** and **P2** with a one-to-one stoichiometry between electrons and protons. As the quinone to hydroquinone redox conversion involves two electrons (see Scheme 3) and since it is well known that the semiquinone state is unstable with respect to disproportionation in water solution we attribute the quinone peak to a $2e2H$ redox process.

The standard potentials (E^0) for the quinone reduction in the polymers were evaluated by extrapolating the pH-dependent lines in Figure 7 to pH 0. For **P1** and **P2** the formal potential was calculated to 0.70 V and 0.63 V, respectively. The higher formal potential of **P1** is likely due to the alkyne in direct conjugation with the quinone moiety. An alkyne linker has previously resulted in a higher formal potential for a different CRP [29]. A battery with **P1** as cathode material would have a higher voltage than with **P2** as cathode material, if combined with the same anode material.

3.6 Mass changes during redox conversion

The frequency change recorded during cycling on the EQCM crystal was converted to mass change using the Sauerbrey equation (Equation 2),

$$\Delta m = \Delta f \frac{A(\rho_q \times \mu_q)^{1/2}}{2(Fq^2)} \quad (2)$$

where Δm is the mass change, Δf is the frequency change, Fq is the reference frequency, A is the area of the active surface, ρ_q is the quartz crystal density, and μ_q is the AT-cut quartz constant. Thin films were used to ensure the validity of the Sauerbrey equation. The mass change was plotted against charge, resulting in linear regions for which slopes could be calculated. Multiplying the slope values (in g/C) with the Faraday constant (96 485 C/mol) gave molecular weight values (g/mol).

The mass changes for both **P1** and **P2** show three linear regions per oxidation and reduction sweep. Two regions correspond to polymer doping (gray fields in Figure 8a and Figure 8b) and one region correlates with the quinone redox chemistry (blue fields in Figure 8a and Figure 8b). The mass per charge changes in the different regions are listed in Table 1. During polymer doping, i.e. in the potential regions on both sides of the quinone redox reaction, the average apparent mass change per mole charge is 22 g/mol. None of the values in Table 1 correspond to the mass of nitrate ($M_w = 62$ g/mol) or any other anion in the electrolyte. The charge compensating process during polymer doping must therefore involve a mixture of nitrate uptake and cation expulsion. Given the acidic conditions used it is likely that proton diffusion dominates the cation expulsion process. Under this assumption, and given that no solvent molecules are involved in the mass transport, 37% of the charges are balanced by

anion uptake while 63% are balanced by expulsion of protons initially present in the polymer during oxidation. During polymer reduction the opposite mass transport processes are occurring. In the potential region where the quinone is redox active the current is dominated by the quinone redox chemistry and the mass is changing with ± 3 grams per mole charge for **P1** and ± 2 grams per mole charge for **P2** (see Table 1). A mass decrease of ~ 1 g/mol indicates, for oxidation, a proton leaving the polymer for each electron leaving, as would be expected when the hydroquinone is oxidized to benzoquinone (see Scheme 3). Interestingly, the small mass changes also indicate that the hydroquinone-to-quinone redox conversion involves only very modest amounts of solvent motion. Together with the mixed anion-cation mass transport during polymer doping it is therefore likely that the polymer film does not experience large volume changes in the potential region investigated since i) solvent molecules are unlikely to be involved during the pendant group redox chemistry and ii) polymer doping involves a small net change in number of ions in the polymer matrix. Based on the deposited mass on the EQCM electrode and the corresponding capacity of the polymer layers the specific capacities of the polymers were estimated to 101 mAh/g (54 % of theoretical capacity) for **P1** and to 77 mAh/g (49 % of theoretical capacity) for **P2**. (Note, however, that the mass used for normalization is based on the total deposited mass and energy dispersive X-ray spectroscopy experiments (see Supplementary Data) indicate a high salt concentration from polymerization that results in low specific capacities compared to the theoretical capacities of the polymers).

3.7 In-situ Conductance

The use of a “water-in-salt” electrolyte enables conductivity measurements below the traditional water stability window. The dependence of conductivity with polymer doping over

an extended potential window, covering the onset of polymer doping (Figure 9c and Figure 9d), can thus be investigated. For both polymers there is a sharp sigmoidal increase in conductance on going from the neutral state of the polymer to the oxidized/doped state, as is commonly seen for unsubstituted PEDOT. The inflection points for oxidation (blue dashed line in Figure 9c) and reduction (red dotted line in Figure 9c) of **P1** are 0.094 V and -0.028 V, respectively, and the inflection points for oxidation (blue dashed line in Figure 9d) and reduction (red dotted line in Figure 9d) of **P2** are 0.01 V and -0.03 V, respectively. The similarity in conductivity onset potentials indicates that the polymer backbones in **P1** and **P2** are quite similar. However, the conductance hysteresis in **P1** (0.12 V) is significantly larger than the hysteresis in **P2** (0.04 V) indicating that **P1** undergoes more significant structural changes upon polymer doping. Moreover, the conductance plateau, that follows the sigmoidal increase at higher potentials, is also higher for **P2** than for **P1**, indicating that **P2** has a higher intrinsic conductivity than **P1**. The increased conductance seen in **P2** could plausibly account for the faster kinetics seen for this polymer as a high conductance indicates an increased degree of ordered regions. This would lead to an increased number of contacts between ordered and amorphous regions in the polymer and hence result in an enhanced coupling constant.

For both polymers a favorable polymer-pendant group redox matching is evident since the quinone redox reaction (Figure 9a and Figure 9b) occurs in a potential region where the polymer is conducting. Although the conductance is largely unaffected by the pendant group redox chemistry, the conductivity of **P1** displays a slight conductance decrease over the quinone peak, Figure 9c. Similar, but much more dramatic effects of the pendant group redox chemistry on polymer conductance have previously been reported for quinone substituted PPy, and it was shown that this polymer-pendant group interaction was reduced by the use of

a longer linker between the two moieties [29]. This effect also accounts for the results in this work where **P1**, with a short linker, exhibits a small but noticeable perturbation of the polymer conductance from the pendant group while **P2** shows no effect of the pendant group redox chemistry. With the longer and more flexible linker the conductivity of the conducting polymer backbone in **P2** has been decoupled from the quinone redox reaction, as can be seen in Figure 9. We therefore propose that the more rigid PEDOT backbone, as compared to PPy, is a better option for the construction of CRP based battery materials with quinone pendant groups.

4 Conclusions

In this report we describe synthesis and electrochemical characterization of two PEDOT based CRPs incorporating hydroquinone pendant groups, with particular emphasis of their use as electrode materials in secondary battery applications. Successful combination of conducting polymers with redox active pendant groups relies on the achievement of i) redox matching between the polymer backbone and the pendant group and ii) the preservation of the individual properties of the two active units, i.e. the intrinsic electronic conductivity of the polymer backbone and the well-defined redox chemistry and high charge storage capacity of the pendant group. In this report we show that both these criteria are met in both polymers. In addition we demonstrate that the materials undergo quite modest mass changes due to a mixed anion-cation mass transport during polymer doping and exclusive charge compensation by proton transport during quinone redox conversion. Taken together we conclude that CRPs based on PEDOT with quinone pendant groups provide a promising material for electrical energy storage applications.

Acknowledgements

Maria Vall is gratefully acknowledged for her assistance with the SEM images. This work was founded by the Swedish Foundation for Strategic Research (SSF), the Swedish Research Council (VR), the Carl Trygger Foundation, the Olle Engqvist Byggmästare Foundation, the Swedish Energy Agency, and the European Union's Horizon 2020 Programme (H2020/2014-2020) under grant agreement n° 644631 (ROLL-OUT).

References

- [1] J.B. Goodenough, Y. Kim, Challenges for Rechargeable Li Batteries, *Chem. Mater.*, 22 (2010) 587-603.
- [2] M. Armand, J.-M. Tarascon, Building better batteries, *Nature*, 451 (2008) 652-657.
- [3] H. Chen, M. Armand, G. Demailly, F. Dolhem, P. Poizot, J.M. Tarascon, From Biomass to a Renewable LiXC₆O₆ Organic Electrode for Sustainable Li - Ion Batteries, *ChemSusChem*, 1 (2008) 348-355.
- [4] W. van Schalkwijk, B. Scrosati, *Advances in Lithium-Ion Batteries*, Kluwer Academic Publishers, New York, 2002.
- [5] L. Suo, O. Borodin, T. Gao, M. Olguin, J. Ho, X. Fan, C. Luo, C. Wang, K. Xu, "Water-in-salt" electrolyte enables high-voltage aqueous lithium-ion chemistries, *Science*, 350 (2015) 938-943.
- [6] Y. Gao, M.V. Yakovleva, W.B. Ebner, Novel LiNi_{1-x}Ti_x/2Mg_x/2O₂ Compounds as Cathode Materials for Safer Lithium - Ion Batteries, *Electrochem. Solid-State Lett.*, 1 (1998) 117-119.
- [7] H.D. Abruña, Y. Kiya, J.C. Henderson, Batteries and electrochemical capacitors, *Physics Today*, 61 (2008) 43-47.
- [8] B. Huskinson, M.P. Marshak, C. Suh, S. Er, M.R. Gerhardt, C.J. Galvin, X. Chen, A. Aspuru-Guzik, R.G. Gordon, M.J. Aziz, A metal-free organic-inorganic aqueous flow battery, *Nature*, 505 (2014) 195-198.
- [9] K. Zhang, C. Guo, Q. Zhao, Z. Niu, J. Chen, High - Performance Organic Lithium Batteries with an Ether - Based Electrolyte and 9,10 - Anthraquinone (AQ)/CMK - 3 Cathode, *Adv. Sci.*, 2 (2015).
- [10] J. Geng, J.-P. Bonnet, S. Renault, F. Dolhem, P. Poizot, Evaluation of polyketones with N-cyclic structure as electrode material for electrochemical

- energy storage : case of tetraketopiperazine unit, *Energy Environ. Sci.*, 3 (2010) 1929-1933.
- [11] H. Nishide, K. Oyaizu, Toward Flexible Batteries, *Science*, 319 (2008) 737-738.
- [12] H.K. Song, G.T.R. Palmore, Redox - Active Polypyrrole: Toward Polymer - Based Batteries, *Adv. Mater.*, 18 (2006) 1764-1768.
- [13] Y. Xuan, M. Sandberg, M. Berggren, X. Crispin, An all-polymer-air PEDOT battery, *Org. Electron.*, 13 (2012) 632-637.
- [14] K. Nakahara, S. Iwasa, M. Satoh, Y. Morioka, J. Iriyama, M. Suguro, E. Hasegawa, Rechargeable batteries with organic radical cathodes, *Chem. Phys. Lett.*, 359 (2002) 351-354.
- [15] K. Koshika, N. Sano, K. Oyaizu, H. Nishide, An ultrafast chargeable polymer electrode based on the combination of nitroxide radical and aqueous electrolyte, *Chem. Commun.*, (2009) 836-838.
- [16] K. Nakahara, K. Oyaizu, H. Nishide, Organic Radical Battery Approaching Practical Use, *Chem. Lett.*, 40 (2011) 222-227.
- [17] S.J. Visco, L.C. DeJonghe, Ionic Conductivity of Organosulfur Melts for Advanced Storage Electrodes, *J. Electrochem. Soc.*, 135 (1988) 2905-2909.
- [18] T. Sotomura, H. Uemachi, K. Takeyama, K. Naoi, N. Oyama, New organodisulfide—polyaniline composite cathode for secondary lithium battery, *Electrochim. Acta*, 37 (1992) 1851-1854.
- [19] M.F. Hohmann-Marriott, R.E. Blankenship, Evolution of Photosynthesis, *Annu. Rev. Plant Biol.*, 62 (2011) 515-548.
- [20] M. Yao, S.-i. Yamazaki, H. Senoh, T. Sakai, T. Kiyobayashi, Crystalline polycyclic quinone derivatives as organic positive-electrode materials for use in rechargeable lithium batteries, *Mater. Sci. Eng., B*, 177 (2012) 483-487.
- [21] H. Alt, H. Binder, A. Köhling, G. Sandstede, Investigation into the use of quinone compounds-for battery cathodes, *Electrochim. Acta*, 17 (1972) 873-887.
- [22] D.R. Ort, C.F. Yocum, *Oxygenic Photosynthesis: The Light Reactions*, Kluwer Academic Publishers, Dordrecht, The Netherlands, 1996.
- [23] S. Er, C. Suh, M.P. Marshak, A. Aspuru-Guzik, Computational design of molecules for an all-quinone redox flow battery, *Chem. Sci.*, 6 (2015) 885-893.
- [24] T. Le Gall, K.H. Reiman, M.C. Grossel, J.R. Owen, Poly(2,5-dihydroxy-1,4-benzoquinone-3,6-methylene): a new organic polymer as positive electrode material for rechargeable lithium batteries, *J. Power Sources*, Volumes 119-121 (2003) 316-320.
- [25] Z. Lei, W. Wei-kun, W. An-bang, Y. Zhong-bao, C. Shi, Y. Yu-sheng, A MC/AQ Parasitic Composite as Cathode Material for Lithium Battery, *J. Electrochem. Soc.*, 158 (2011) A991-A996.
- [26] Z. Song, H. Zhou, Towards sustainable and versatile energy storage devices: an overview of organic electrode materials, *Energy Environ. Sci.*, 6 (2013) 2280-2301.
- [27] C. Karlsson, A. Gogoll, M. Strømme, M. Sjödin, Investigation of the Redox Chemistry of Isoindole-4,7-diones, *J. Phys. Chem. B*, 117 (2013) 894-901.

- [28] K.S. Park, S.B. Schougaard, J.B. Goodenough, Conducting - Polymer/Iron - Redox - Couple Composite Cathodes for Lithium Secondary Batteries, *Adv. Mater.*, 19 (2007) 848-851.
- [29] C. Karlsson, H. Hao, M. Strømme, A. Gogoll, M. Sjödin, Impact of linker in polypyrrole/quinone conducting redox polymers, *RSC Adv.*, 5 (2015) 11309-11316.
- [30] X. Huang, L. Yang, R. Emanuelsson, J. Bergquist, M. Strømme, M. Sjödin, A. Gogoll, A versatile route to polythiophenes with functional pendant groups using alkyne chemistry, *Beilstein J. Org. Chem.*, 12 (2016) 2682-2688.
- [31] R. Emanuelsson, M. Sterby, M. Strømme, M. Sjödin, An all-organic proton battery Submitted manuscript, (2017).
- [32] C. Karlsson, H. Huang, M. Strømme, A. Gogoll, M. Sjödin, Ion- and Electron Transport in Pyrrole/Quinone Conducting Redox Polymers Investigated by In Situ Conductivity Methods, *Electrochim. Acta*, 179 (2015) 336-342.
- [33] E. Laviron, General expression of the linear potential sweep voltammogram in the case of diffusionless electrochemical systems, *J. Electroanal. Chem. Interfacial Electrochem.*, 101 (1979) 19-28.
- [34] A.J. Bard, L.R. Faulkner, *Electrochemical Methods: Fundamentals and Applications*, 2nd ed., John Wiley & Sons, New York, NY, 2001.
- [35] R. Noriega, J. Rivnay, K. Vandewal, F.P.V. Koch, N. Stingelin, P. Smith, M.F. Toney, A. Salleo, A general relationship between disorder, aggregation and charge transport in conjugated polymers, *Nat. Mater.*, 12 (2013) 1038-1044.

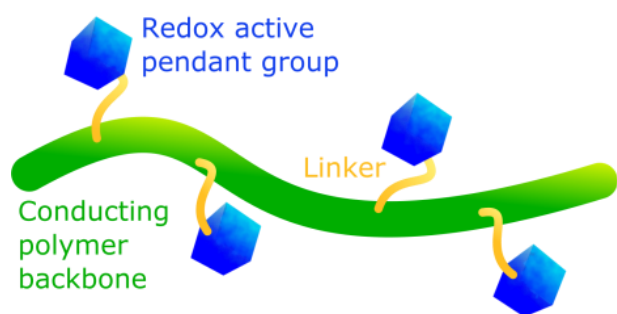


Figure 1. Schematic picture of a conducting redox polymer.

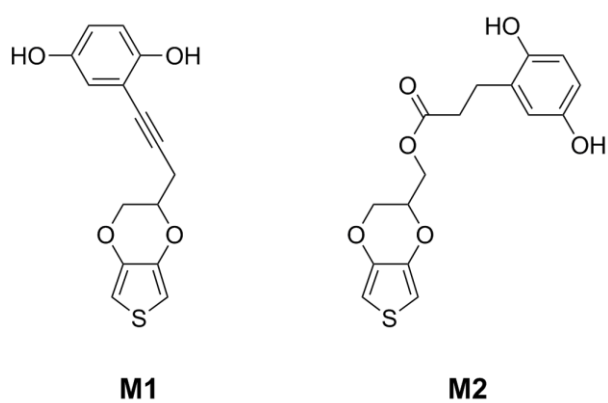


Figure 2. Chemical structures of the monomers (**M1**) and (**M2**), which subsequently were electropolymerized to polymer **P1** and **P2**, respectively.

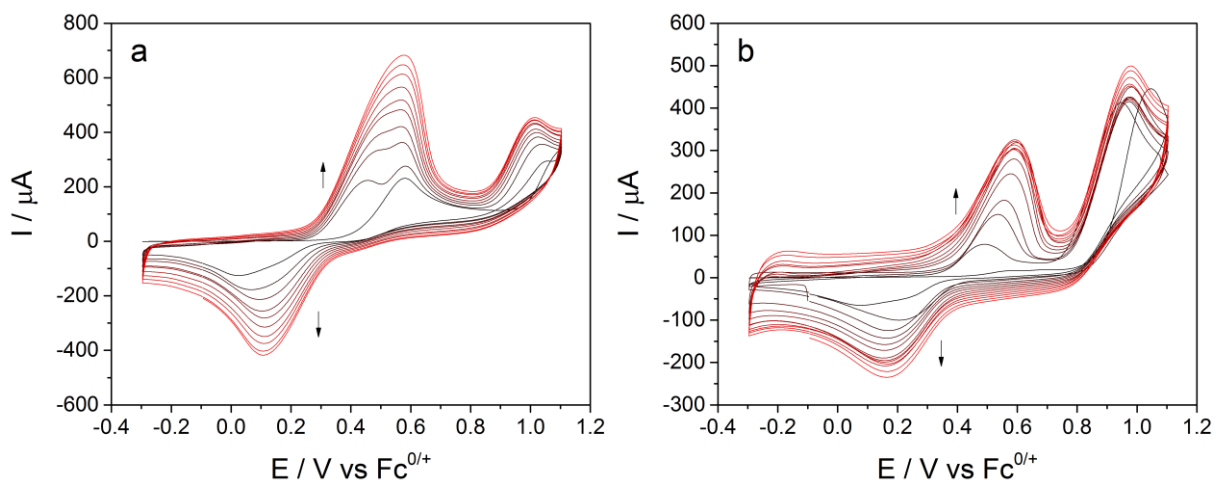


Figure 3. Electropolymerization of a) **M1** (10 scans, forming polymer **P1**) and b) **M2** (13 scans, forming polymer **P2**) onto GC electrodes with a scan rate of 100 mV/s. Monomers (5 mM) were dissolved in dry MeCN containing 0.1 M TBAPF₆.

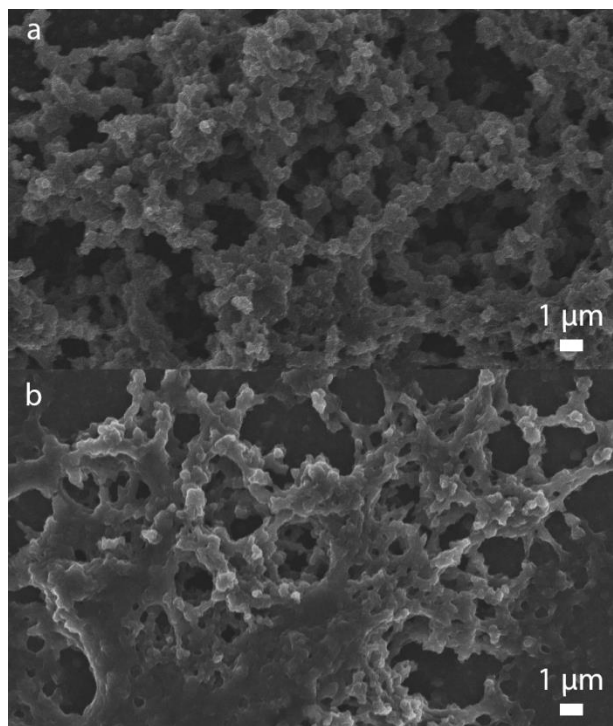


Figure 4. SEM image at 10,000 x magnification of a) **P1** and b) **P2** electropolymerized on a graphite paper.

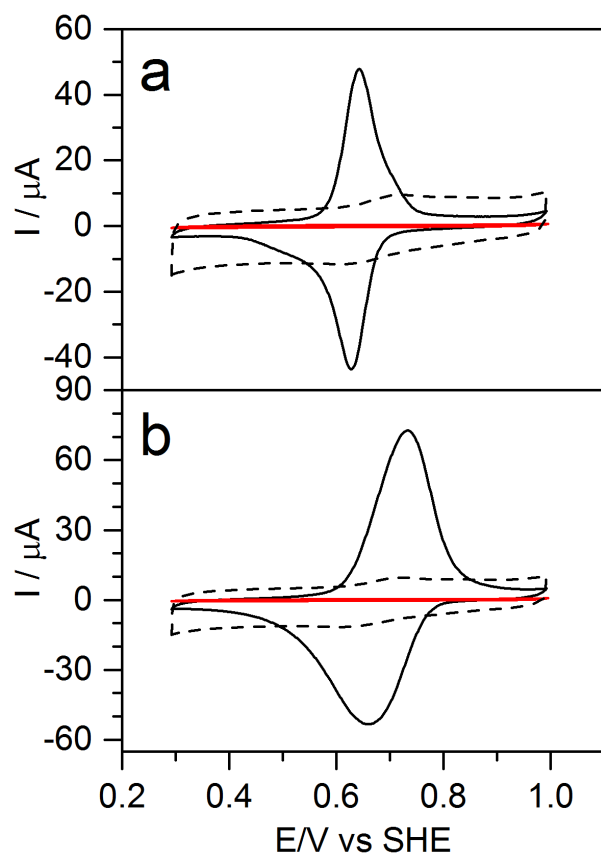


Figure 5. CV of a) **P1** and b) **P2** characterized in aqueous NaNO_3 buffer (pH 0) at a scan rate of 25 mV/s. Red lines correspond to an empty GC electrode and black dashed lines correspond to a PEDOT covered electrode used for comparison.

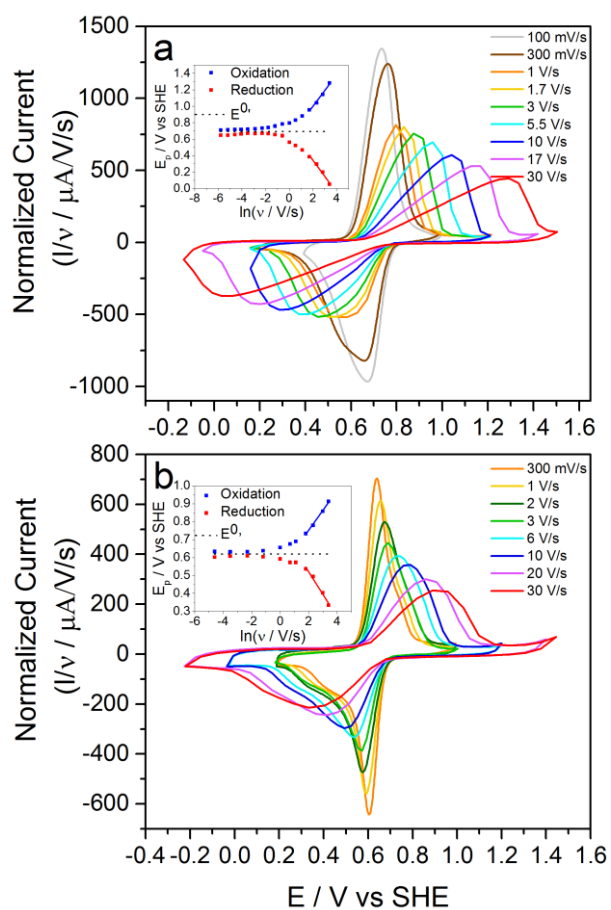


Figure 6. a) CVs of **P1** at scan rates between 0.1 V/s and 30 V/s. b) CVs of **P2** at scan rates between 0.3 V/s and 30 V/s. The insets show the peak potential dependence on scan rate. From the linear regions the apparent rate constants were for **P1** calculated to 7.8 s^{-1} for oxidation and to 6.4 s^{-1} for reduction and for **P2** the rate constants were calculated to 20.3 s^{-1} for oxidation and to 26.7 s^{-1} for reduction. Characterized in aqueous NaNO_3 buffer (pH 0).

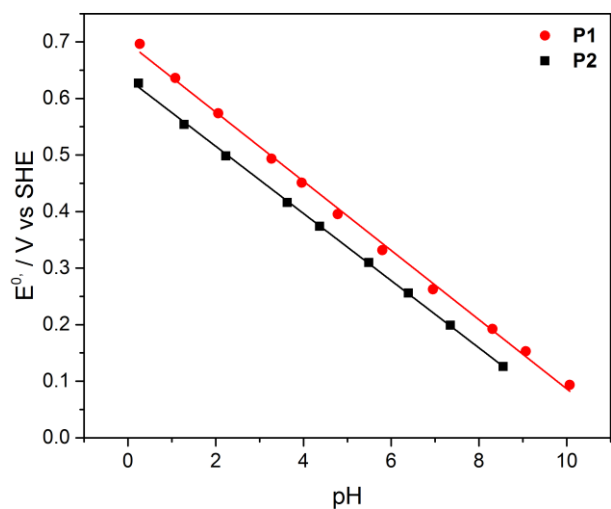


Figure 7. pH dependence of **P1** (red circles) and **P2** (black squares). Characterized in aqueous NaNO₃ buffer at a scan rate of 10 mV/s. pH adjusted with NaOH and HNO₃.

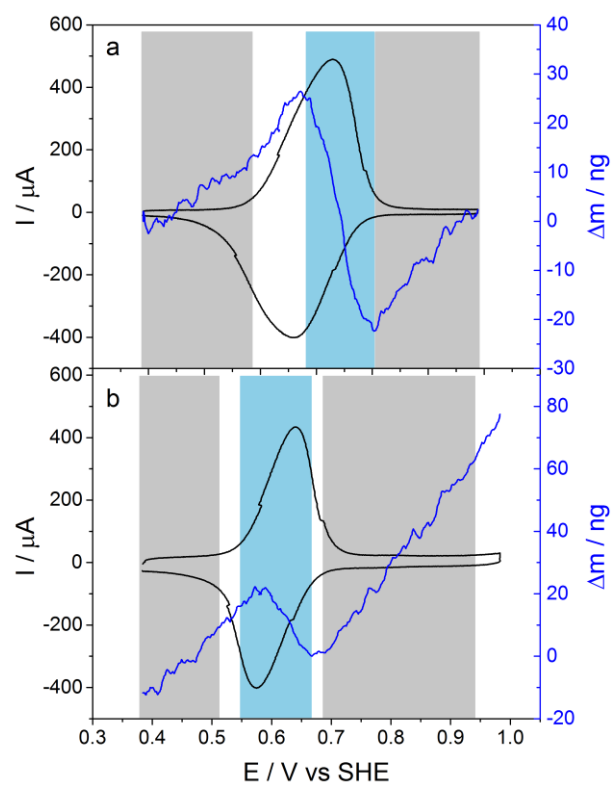


Figure 8. a) EQCM data for **P1**. b) EQCM data for **P2**. Mass change during an oxidation sweep is shown. Gray regions show oxidative doping of the PEDOT backbone (ca +22 g/mol) and blue region shows oxidation of the quinone pendant group (-2 g/mol). Characterized in aqueous NaNO₃ buffer (pH 0) at a scan rate of 25 mV/s.

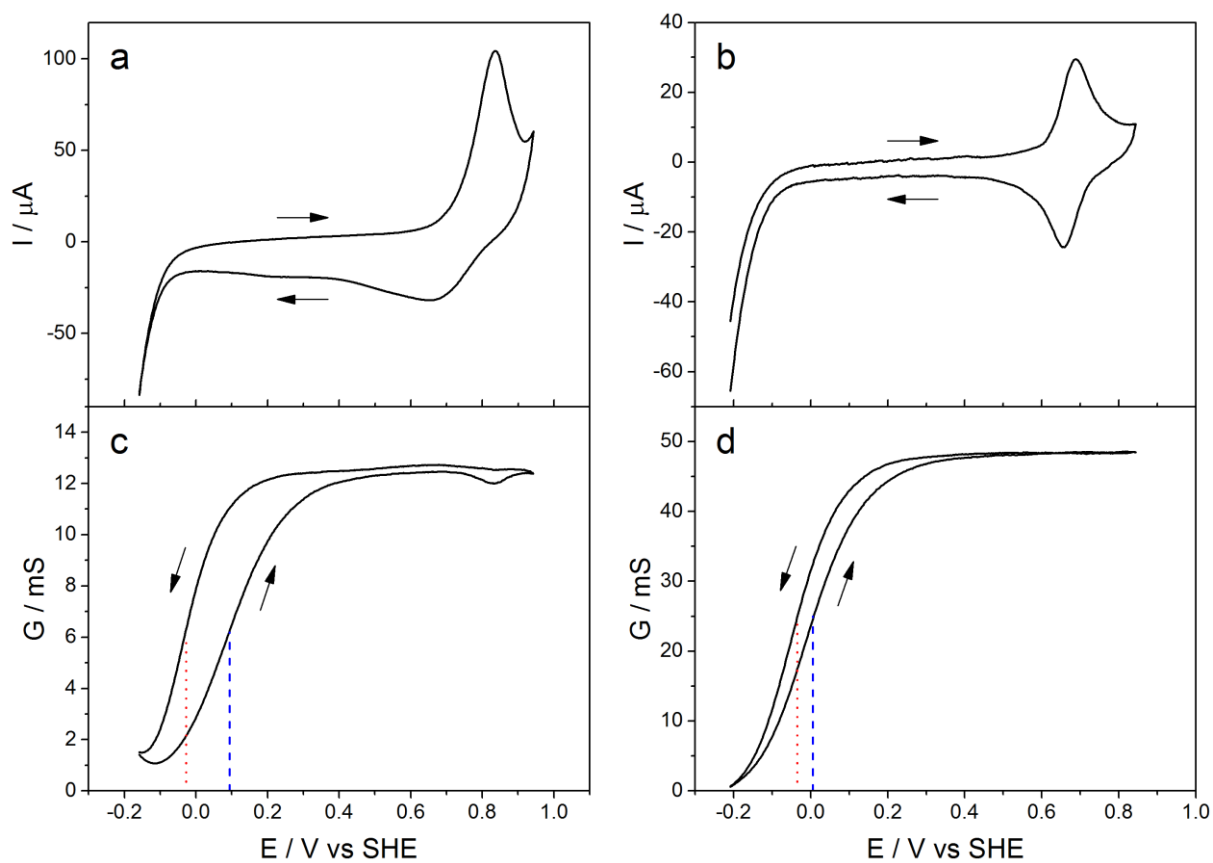
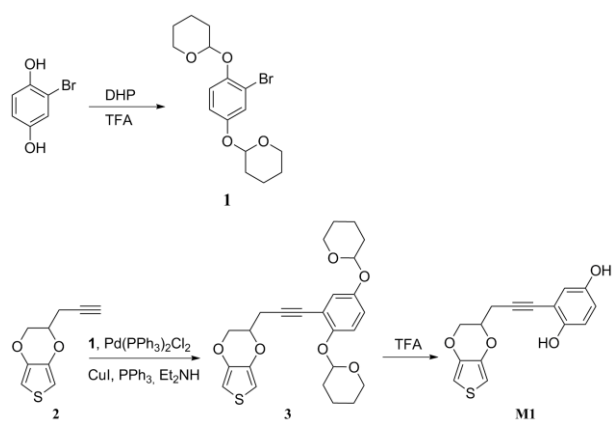
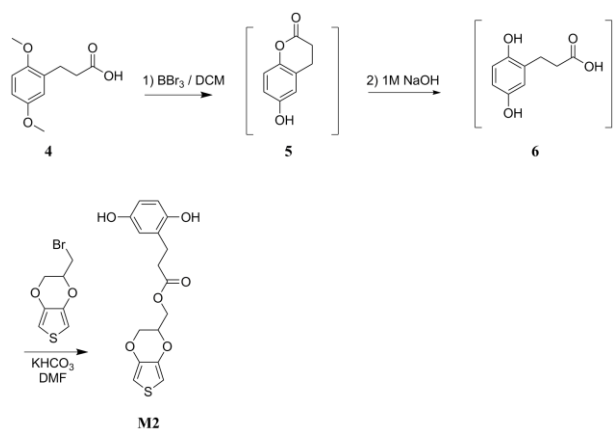
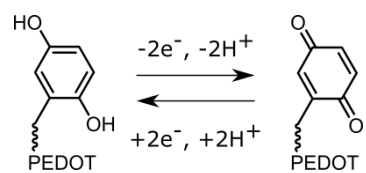


Figure 9. CV of a) **P1** and b) **P2**, and conductance data for c) **P1** and d) **P2**. The red dotted line marks inflection points for reduction and the blue dashed line marks inflection points for oxidation. Measurements performed in a sodium chloride and hydrochloric acid (1 M) salt slurry at a scan rate of 10 mV/s at 22 °C, using an IDA electrode.

Scheme 1. Synthetic route to **M1**.Scheme 2. Synthetic route to **M2**.

Scheme 3. Oxidation/reduction of hydroquinone/benzoquinone.

Table 1. Mean molecular weight of molecules added to and/or expelled from the polymer films during a CV experiment.

	M_w (g/mol)		
	Lower potential region	Quinone region	Higher potential region
Oxidation of P1	+18	-3	+25
Reduction of P1	-6	+3	-27
Oxidation of P2	+20	-2	+21
Reduction of P2	-20	+2	-36